Development of Hot Spots and Ignition Behind Reflected Shocks in $2\mathrm{H_2} + \mathrm{O_2}$

A. Khokhlov
The University of Chicago, Chicago, Illinois, USA
J. Austin and A. Knisely
The University of Illinois at Urbana-Champaign, Urbana-Champaign, Illinois, USA

The goal of this work is a numerical study of the hot spots leading to mild and strong ignition behind reflected shocks in reactive gases. To this end we carry out three-dimensional reactive flow Navier-Stokes (NS) direct numerical simulations (DNS) of the shock reflection in stoichiometric $2H_2 + O_2$ mixture. We find that the formation of hot spots responsible for the *transition* between strong and mild ignition regimes may be related to the generation of acoustic (pressure) waves in the recirculation region of the bifurcated reflected shock. The subsequent modulation of the reflected shock by the pressure waves creates secondary entropy perturbations in the shocked matter which serve as initial sites for the hot spot development. The shock Mach number, M, determines the average temperature of the shocked matter and controls whether the ignition leads directly to a detonation (strong ignition) or to a number of growing flame kernels and a mild ignition.

1 Introduction

Strong and weak ignition regimes were first observed in reflected shock tube experiments in $2H_2 + O_2$ in [1, 2]. For sufficiently strong shocks the ignition occurs at the end wall of the tube and leads to an immediate onset of a detonation wave (strong ignition). With decreasing M the ignition moves away from the wall and takes place in hot spots which form multiple flame kernels. The flame kernels merge and give rise to a detonation at a later time (mild ignition). The transition between the two regimes was associated with the second explosion limit in $2H_2 + O_2$ in [1]. In [3] it was found that the transition roughly corresponds to $(\partial\tau/\partial T)_{tr} \simeq -2\ \mu sec/K$, where τ is the induction time; strong ignition occurs when $(\partial\tau/\partial T) < (\partial\tau/\partial T)_{tr}$. In [4] this was theoretically interpreted as a necessary condition on the temporal coherence of the explosions of individual hot spots. The well-known Zeldovich gradient or SWACER detonation criterion requires a spontaneous reaction front to propagate with the phase velocity $(\partial\tau/\partial x)^{-1} \approx a_s$, where a_s is the local sound speed. This translates into a similar necessary condition $(\partial\tau/\partial T) < (\partial\tau/\partial T)_{tr}$ with $(\partial\tau/\partial T)_{tr} \approx (a_s|\nabla T|)^{-1}$. Neither criteria however provide a full description of the ignition process. In particular, the critical value of $(\partial\tau/\partial T)_{tr}$ cannot be derived theoretically because the origin, location, and distribution of physical parameters inside the hot spots are generally unknown. The goal of this work is a numerical study of the origin and evolution of hot spots leading to mild and strong ignition regimes.

2 Formulation

Our problem is described by the compressible reactive flow Navier-Stokes (NS) equations of fluid dynamics,

$$\partial\rho/\partial t = -\nabla\cdot(\rho\mathbf{u}), \tag{1}$$

$$\partial\rho\mathbf{u}/\partial t = -\nabla\cdot\left(\rho\mathbf{u}\otimes\mathbf{u} + P\hat{\mathbf{I}} + \hat{\pi}\right), \tag{2}$$

$$\partial E/\partial t = -\nabla\cdot\left(\mathbf{u}\,(E+P) + \mathbf{u}\cdot\hat{\pi} + \mathbf{q}^e\right), \tag{3}$$

$$\partial\rho Y_i/\partial t = -\nabla\cdot\left(\rho\left(\mathbf{u}+\mathbf{u}^i\right)Y_i\right) + \rho\dot{w}_i, \quad i = 1,...,N, \tag{4}$$

for the mass density, ρ, fluid velocity $\mathbf{u}$, total energy density $E = \rho e + \frac{1}{2}\rho u^2$, and mass fractions of the reactants, Y_i, where e is the internal energy per unit mass, P is the pressure, $\mathbf{u}^i$ are the diffusion velocities of reactants, $\hat{\pi} = -\mu\left((\nabla\mathbf{u}) + (\nabla\mathbf{u})^T - (2/3)(\nabla\cdot\mathbf{u})\hat{\mathbf{I}}\right)$ is the viscous stress tensor, $\mathbf{q}^e = -\lambda\nabla T + \rho\sum h_i\mathbf{u}^i$ is the diffusion energy flux, μ is the physical viscosity, λ is the thermal conductivity, h_i are the enthalpies of the reactants, and $\dot{w}_i$ are the chemical reaction terms. We used the kinetic scheme of [5] with $N = 8$ reactants, H, H_2, O, O_2, OH, H_2O, HO_2, and H_2O_2, and the NASA seven-terms polynomial equation of state [6]. Diffusion velocities $\mathbf{u}^i$ were found from the Stefan-Maxwell

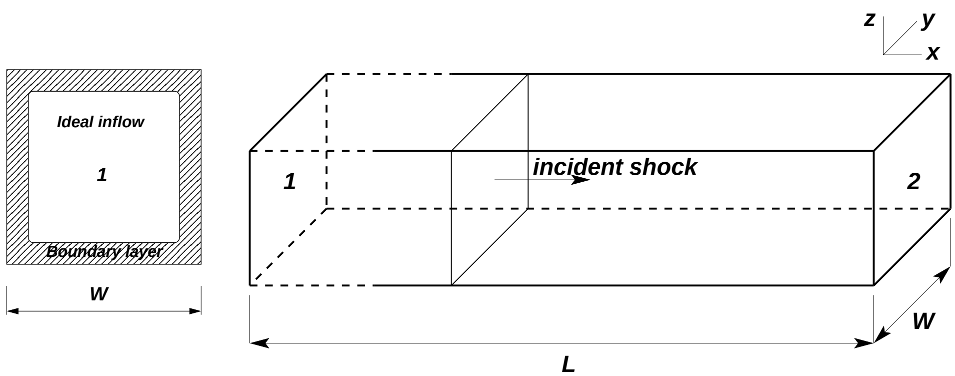

Figure 1: Right - computational domain, 1 - inflow, 2 - end wall. Left - inflow boundary conditions: white area - ideal post-shock inflow, dashed area - post-shock boundary layer.

(SM) equations, which were solved exactly [10]. The multi-species viscosity, thermal conductivity, binary diffusion coefficients, and thermal diffusion ratios were calculated following [**?**, 7–9]. The Navier-Stokes equations were integrated using a second-order accurate, conservative, Godunov-type, adaptive mesh refinement code [11]. Euler fluxes were calculated using a Riemann solver and a monotone Van Leer reconstruction. The diffusion fluxes were calculated using second-order central differencing. The reaction terms were integrated together with the energy equation using an unconditionally stable stiff integration method with sub-sycling. The computational setup is shown in Figure 1. The non-slip isothermal boundary conditions were used at solid walls. The inflow boundary was described by the ideal post-shock inflow conditions in the middle of the tube and the self-similar growing boundary layer solution near the walls. The self-similar profiles were pre-computed using viscosity, thermal conductivity, and mass diffusion described above.

3 Shock reflection

Figures 2 - 4 show results of a simulation of a shock reflection in a tube with $W = 5$cm, for $M = 2.72$, ambient pressure $P = 0.39$ atm, and ambient temperature $T = 300$K. The numerical resolution was

$\Delta = 6.1$ microns. Size of the problewm was cut by a factor of four by assuming a symmetry with respect to XY and XZ center-planes.

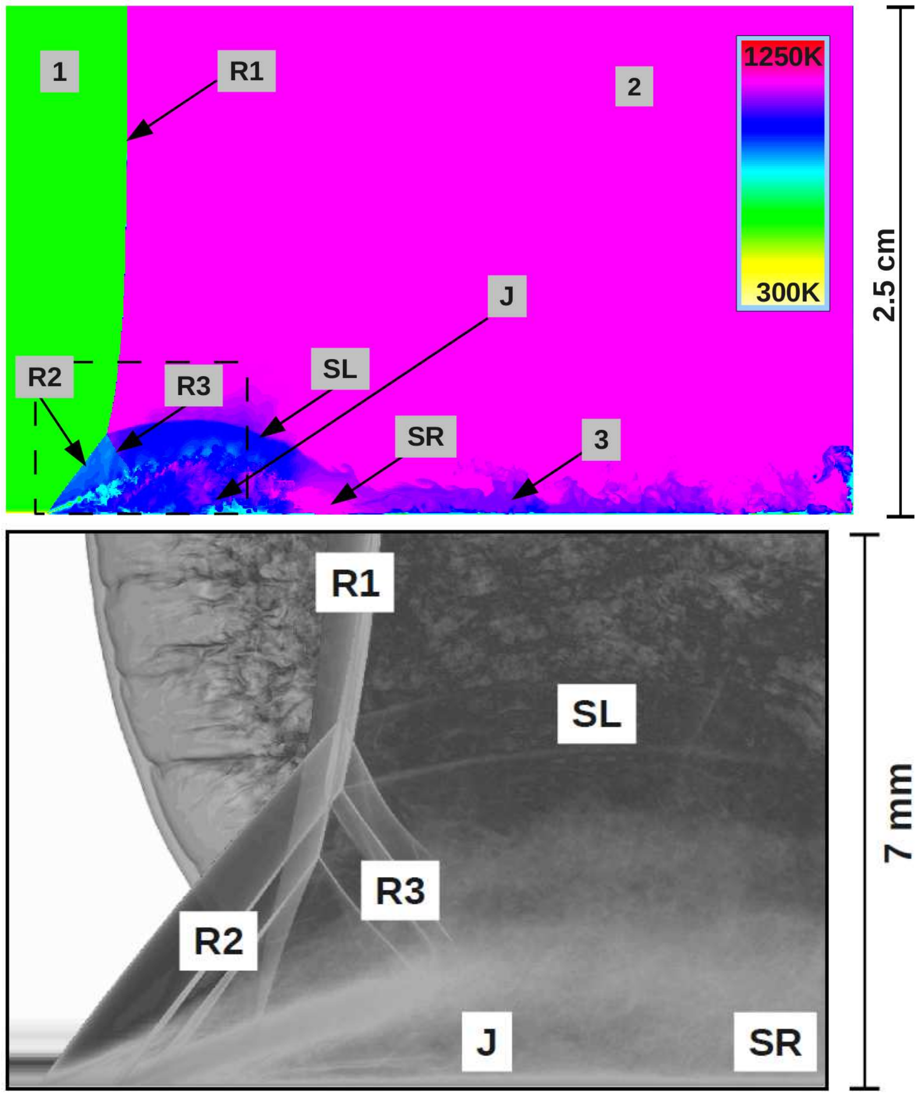

Figure 2: Shock wave reflection in $2H_2 + O_2$. Top - two-dimensional temperature distribution in the center-plane of the tube at $t = 62.80$ μs after reflection. Reflected shock is moving to the left. Bottom - pseudo-schlieren image of the reflected shock area (dashed line).

Fig. 2 illustrates the main features of the reflection. After the incident shock reaches the end wall, the reflected shock, (R1), begins to propagate back to the inflow boundary. Interaction of (R1) with the boundary layer created by the incident shock leads to shock bifurcation and the formation of the λ-structure made of the inclined forward shock (R2) and a secondary shock (R3). In the middle of the tube the matter passes from the region (1) through the (R1) shock into the region (2) where it remains nearly stationary. Close to the walls the incoming matter passes through the shocks (R2) and (R3) and continues to flows towards the end wall under the slip line (SL). Part of the flow is redirected in the stagnation region (SR) into the recirculation jet (J) and begins to move to the left, toward (R2). Remaining matter passes through (SR) and continues to slowly flow through the region (3) toward the end wall. A pseudo-schlieren image of the shock region illustrates a true three-dimensional structure of the reflected shock region with highly distorted (R1) and (R2) shocks, and with multiple secondary shocks.

4 Acoustic and entropy perturbations

The recirculation region behind the reflected shock, (J) and (SR), is violently unstable, contains sonic turbulence, and continuously sheds vortices. The vortex shedding is accompanied by the radiation of acoustic (or pressure) waves. Figure 3 shows the fine structure of the temperature field in the center-plane of the tube for three moments of time. Cylindrical patterns of acoustic waves emanating from the vicinity of (SR) are clearly discernible in the region (2) of the post-shock matter. The waves appear soon after the reflection and eventually they fill the entire space behind the reflected shock. Numerical animation confirms that that circular patterns move through matter with the local sounds speed. In addition to acoustic waves the temperature field also contains clearly visible linear patterns of perturbations which pass through the region (2) at an angle $\alpha \simeq 30$ deg to the shock wave (R1). The animation shows that the linear patterns are nearly stationary – they represent the perturbations of entropy in the region (2). Frames 3a and 3b of Fig. 3 show the T and P fields for the same moment of time. Acoustic waves are visible in both T and P frames but the linear patterns are visible only in the T frame. This is a confirmation that they are associated with the $P = const$ perturbations of entropy. The linear pattern of the entropy perturbations admits a simple explanation. As evidenced by Fig. 3a, the entropy perturbations originate at the shock wave when the shock is modulated by the arriving acoustic waves. Let U_s be the velocity of (R1) shock with respect to the tube and U_a be the phase velocity of acoustic waves along the surface of the shock. The instantaneous angle of the generated linear pattern is given by $\tan(\alpha) = U_s/U_a$. The phase velocity of acoustic waves at a given interaction point on the shock surface is $U_a = a_s/\cos\beta$, where a_s is the local sound speed in region (2) and β is the direction from the point of interaction to the source of acoustic waves, which is (SR). Combining the two formulas leads to

$$\alpha = \arctan\left(\left(\frac{U_s}{a_s}\right)\cos\beta\right) \qquad (5)$$

In our case $U_s = 590$ m/s, $a_s = 1040$ m/s, and $(\frac{U_s}{a_s}) = 0.57$. For large distances from (SR) $\beta \to 0$ and the inclination angle asymptotes to $\alpha \simeq \arctan(0.57) = 29.7$ deg, in a good agreement with Fig. 3. When β increases the inclination angle α must decrease. The maximum value of β roughly corresponds to a direction from (SR) to the tip of the λ-structure, which is $\beta \simeq 60$ deg in our case. The corresponding inclination

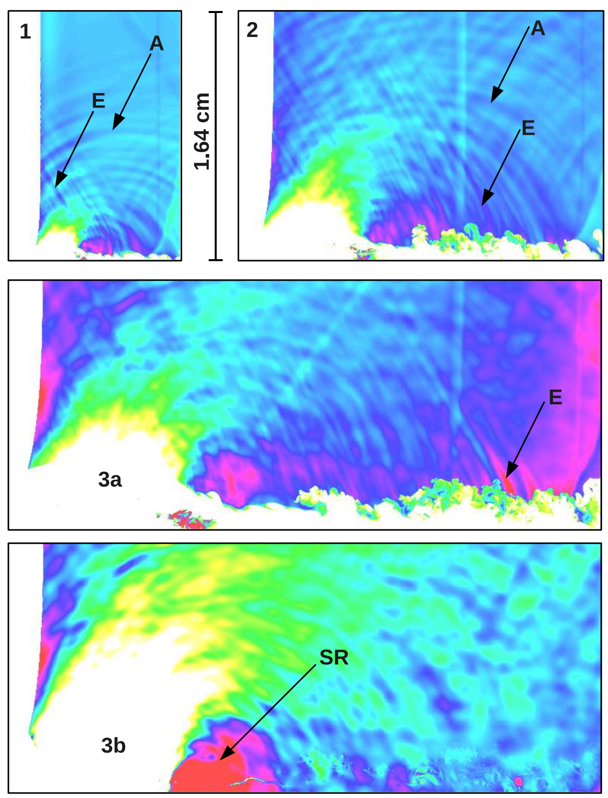

Figure 3: Acoustic (A) and entropy (E) perturbations behind the reflected shock. Frames (1), (2) and (3a) show the center-plane temperature in a narrow range $1130 - 1170$ K at $t = 16.37$ μs, $t = 37.62$ μs, and $t = 62.80$ μs after reflection. Frame (3b) shows P at $t = 62.80$ μs in the narrow range of $14.8 - 15.8$ atm.

$\alpha \simeq 15$ deg given by (5) is in a reasonable
agreement with the smaller inclination angles of the entropy perturbations observed near the side wall, see Fig. 3.

5 Ignition of hot spots

The entropy perturbations are the preferential sites for the development of the hot spots because they provide a persistent environment with an elevated temperature at which chemical reactions may proceed faster. Temperature in acoustic waves oscillates around its mean value with positive and negative temperature fluctuations nearly compensating each other. The same holds for the recirculation region itself. The temperature fluctuations in the stagnation region reached in our case $\simeq 1200$K but the residence time of the fluid elements in this region is short and the reactions have a very limited time to proceed. In the simulations the hot spots developed at the sites of the largest and the earliest entropy perturbations located in region (2) in close proximity of the side walls but separated from the walls by the flow of colder gas in the region (3). Figure 4 shows images of the hot spot ignition which took place $\simeq 0.5$ cm from the end wall and near the corner formed by the two side walls of the tube. The ignition of the hot spots gave rise to flame kernels shown in Fig. 4a,b. The visible flame velocity estimated from the simulation was $\simeq 300$ m/s, which translates to a flame velocity $S \simeq 30 - 40$ m/s relative to matter. The flame propagated in the nearly $P \simeq const$ regime with average $P \simeq 25$ atm and $\simeq 20\%$ pressure variations across the kernels. The slightly elevated pressure ahead of the growing flame quickly changed the temperature in the surrounding gas and triggered a a detonation visible in Fig. 4c. The expansion velocity of the detonation kernel is $\simeq 1.5$ km/s and the pressure inside the kernel is $P \simeq 180$ atm, significantly larger than that in the surrounding material.

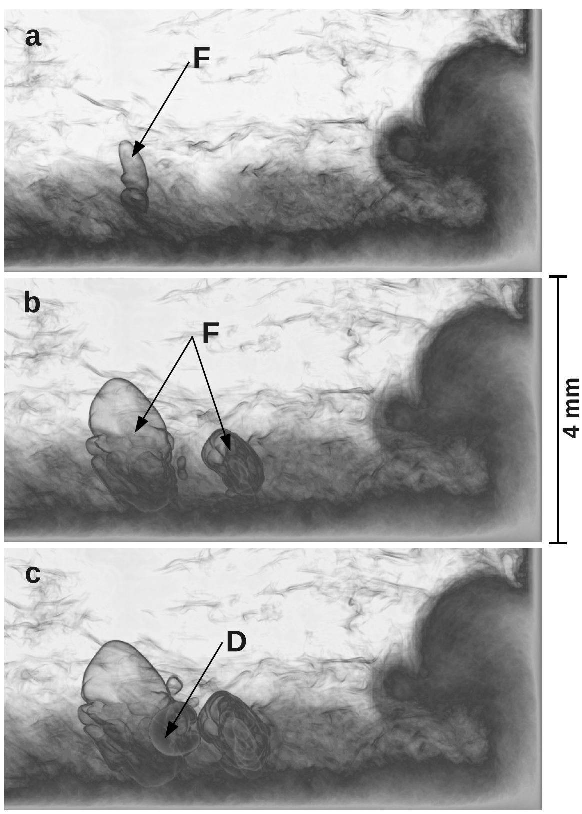

Figure 4: Mild ignition in $2H_2 + O_2$. Numerical pseudo-schlieren images of the lower right corner of the shock tube. F - flame kernels. D - detonation kernel. Times are (a) - 61.38 μs , (b) - 62.62 μs, and (c) - 62.96 μs after shock reflection.

The post-shock temperature in region (2) calculated from by the Hugoniot relations for an ideal reflection is $T_2 = 1156.4$K and the ideal zero-dimensional ignition time delay calculated from the kinetic mechanism is $\tau_i = 62.27$ μs. The ignition time delay foundin the simulations, $\tau \simeq 61$ μs is practically the same. The simulations clearly represent the borderline case of the mild ignition. We found that the shock reflection with $M = 2.75$ leads to a direct initiation of a detonation and strong ignition. On the other hand, simulations with $M = 2.60$, $M = 2.63$, and $M = 2.65$ all resulted in a mild ignition similar to the $M = 2.72$ case described above.

In the present work we neglected the potentially important effects of the slowdown of the incident shock inside the shock tube and the surface chemistry such as the catalytic dissociation of H_2 at the walls. These effects are out of the scope of this paper and will be discussed elsewhere. The main emphasis of this work is the elucidation of the acoustic mechanism of the formation of the entropy perturbations in the reactive gas caused by the interaction of the reflected shock with pressure waves generated by the shock reflection itself. The mechanism is purely hydrodynamical and should operate regardless of other mechanism that may be present. The acoustic mechanism is sufficient for explaining the transition between weak and strong ignition regimes. By its very nature, however, the mechanism is limited to temperatures greater than roughly 1000 K because the secondary entropy perturbations generated by this mechanism are fundamentally limited by the amplitude of the pressure perturbations emitted from the recirculation region and cannot exceed a level of $\simeq$ a few per cent.

Acknowledgement An award of computer time was provided by the Innovative and Novel Computational Impact on Theory and Experiment (INCITE) program. This research used resources of the Argonne Leadership Computing Facility, which is a DOE Office of Science User Facility supported under Contract DE-AC02-06CH11357.

References

[1] Voevodsky, V. V. and Soloukhin, R. I. (1965). On the mechanism and explosion limits of hydrogen-oxygen chain self-ignition in shock waves. Symposium (International) on Combustion, 10:279-283.

[2] R.A. Strehlow and A. Cohen (1962). Initiation of Detonation. Phys. Fluids, 5:97-101.

[3] J.W. Meyer and A.K. Oppenheim (1971). On the shock-induced ignition of explosive gases. Thirteenth Symposium (International) on Combustion, 13:11531164.

[4] J.W. Meyer and A.K. Oppenheim (1971). Coherence theory of the strong ignition limit. Combust. Flame, 17:65-68.

[5] M.O. Conaire and H.J. Curran and J.M. Simmie and W.J. Pitz and C.K. Westbrook (2004). A Comprehensive Modeling Study of Hydrogen Oxidation. Int. J. Chem. Kinet. 36:603–622.

[6] A. Burkat and B. Ruscic (2005). Third Millennium Ideal Gas and Condensed Phase Thermochemical Database for Combustion with Updates from Active Thermochemical Tables, ANL-05/20, Chicago, IL, USA.

[7] J.O. Hirschfelder and C.F. Curtiss and R.B. Bird (1954). Molecular Theory of Gases and Liquids, John Wiley & Sons, Inc., New York.

[8] C.R. Wilke (1950) A Viscosity Equation for Gas Mixtures. The Journal of Chemical Physics, 18:517-519.

[9] E.A. Mason and S.C. Saxena (1958). Approximate Formulas for the Thermal Conductivity of Gas Mixtures. Physics of Fluids, 5:139–146.

[10] V. Giovangigli (1991). Convergent iterative Methods for Multicomponent Diffusion. Impact of Computing in Science and Engineering, 3:244–276.

[11] A. Khokhlov (1988). Fully Threaded Tree Algorithms for Adaptive Refinement Fluid Dynamics Simulations. J. Comput. Phys., 143:519–543.